NANO LETTERS

2008
Vol. 8, No. 2
485−490

Fluorescence Enhancement in Hot Spots of AFM-Designed Gold Nanoparticle Sandwiches

Alpan Bek,[†] Reiner Jansen, Moritz Ringler, Sergiy Mayilo, Thomas A. Klar,*[,‡] and Jochen Feldmann*

Photonics and Optoelectronics Group, Physics Department and CENS, Ludwig-Maximilians-Universität München, Amalienstrasse 54, 80799 Munich, Germany

Received October 9, 2007; Revised Manuscript Received November 26, 2007

ABSTRACT

We observe an enhancement of fluorescence from a single fluorescent sphere, which is sandwiched between two individual gold nanoparticles, forming a hot spot of strong field enhancement. The fluorescence enhancing hot spot is custom-designed by the deliberate assembly of gold nanoparticles with an atomic force microscope cantilever. The fluorescence intensity is monitored while the separation between the two gold nanoparticles is reduced by gradually pushing the gold nanoparticles closer to the fluorescent sphere. The fluorescence enhancement is maximal when the distance between the two gold nanoparticles is smallest, when the excitation polarization is parallel to the axis of the sandwich, and when the fluorescent sphere is positioned exactly on the axis connecting the two gold nanoparticles.

Spontaneous emission of fluorescence can be modified by the resonant coupling of fluorescent molecules to the external electromagnetic environment.[1] Many devices based on modified spontaneous emission have been demonstrated within the past decade.[2,3] Resonant cavities,[4] whispering galleries,[5] photonic crystals,[6] planar metal surfaces[7,8] or metallic nanoparticles[9−12] are examples of devices that modify the electromagnetic environment. Rough metal film surfaces are observed to enhance Raman scattering,[13−18] resonant Raman scattering,[15] and fluorescence from adsorbed molecules.[19,20] Single metal nanoparticles have been reported to decisively influence Raman scattering and fluorescence, as well.[9−12,17] To bridge these two extremes of single nanoparticles and rough films, it is of utmost importance for the understanding of so-called hot spot effects to study simple aggregates of noble metal nanoparticles. The simplest system in which field enhancement effects can be studied is the nanoparticle dimer.[21] The enhancement of Raman scattering in the center of noble metal nanoparticle dimers has been investigated.[22−26] Much less is known about the fluorescence of molecules between two noble metal nanoparticles. Only very recently, reports addressed this question and fluorescence enhancement was found when semiconductor nanocrystals or fluorophores are placed between two metal nano-objects.[27−29] The paired nano-objects were a bowtie antenna fabricated by e-beam lithography[30] or focused ion beam milling,[27] rod-like nanoantennas fabricated by e-beam lithography,[28] or pairs of gold nanoparticles tethered together with DNA of a certain length.[29] With all these techniques, a survey about how the fluorescence enhancement depends on the distance of the two metal nano-objects is in principle possible, but it would require a time-consuming sample preparation for each specific distance, and the fluorescing object would not be identical on each sample.

In contrast to the previously mentioned approaches to form sandwiches of metal nanoparticles, we present targeted fabrication of hot spots by organizing the spatial configuration of plasmonic nanoparticles around a nanosized, spherical, fluorescent bead using atomic force microscopy (AFM) manipulation.[31,32] When a single gold nanoparticle (AuNP) is approached to a fluorescent sphere (FS), the fluorescence decreases by 30% up to a AuNP−FS separation of 90 nm. For an even closer approach, the fluorescence increases to 150% of the original value. Upon the approach of the second gold nanoparticle, the fluorescence increases further to 270%, which is more than the sum of the effects of the two noninteracting AuNPs. Our AFM manipulation also allows us to conveniently design geometries other than the straight AuNP−FS−AuNP sandwich. If, however, the FS is not placed right in line with the connecting axis of the two AuNPs, the fluorescence enhancement is weakened, which proves that the hot spot is formed right between the two AuNPs.

* Corresponding authors. E-mail: thomas.klar@tu-ilmenau.de, jochen.feldmann@physik.uni-muenchen.de.
[†] Present address: CBM, AREA Science Park, Trieste, Italy.
[‡] Present address: Dept. of Physics, TU Ilmenau, Germany.

10.1021/nl072602n CCC: $40.75
Published on Web 01/04/2008

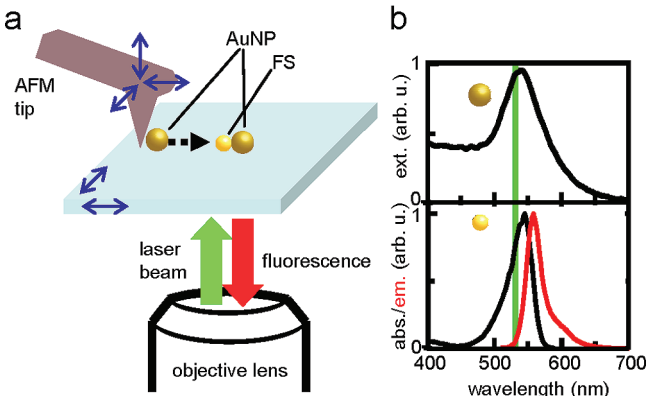

Figure 1. Experimental setup. (a) An AFM is placed on top of a confocal inverted microscope. The AFM is used in noncontact mode for acquiring height images and in contact mode to mechanically push the gold nanoparticles (AuNPs) toward a fluorescent sphere (FS). A 532 nm CW laser source is used to excite the fluorophores in the FS. Fluorescence and AFM images are recorded by raster-scanning the sample while the closed-loop, three-axis scan stage of the AFM head is used to align the AFM tip with the optical axis. (b) The upper panel shows the measured extinction spectrum of a 60 nm Au colloidal solution, exhibiting a plasmon resonance. The lower panel shows the measured absorption (black) and emission (red) spectra of the FSs. The wavelength of the excitation laser is marked as a green vertical line.

The in situ manipulation of the AuNPs and the detection of the fluorescence is realized by an AFM (jpk Instruments) placed on top of an inverted optical microscope (Zeiss) (Figure 1a).[33] In addition to the three closed-loop, piezo-driven axes of the AFM, a two-axis, closed-loop, piezo-driven sample stage is employed. The two lateral scan axes of the AFM head are used to confocalize the AFM tip with the focus of the inverted microscope, while the two-axes sample stage and the vertical feedback piezo of the AFM head are used to perform AFM imaging (in tapping mode) and to laterally push gold nanoparticles lying on the substrate (in contact mode). The beam of an unpolarized laser (532 nm) is expanded and directed into the side port of the microscope. The beam overilluminates the 100×, 1.45 NA oil immersion lens that focuses the laser beam to a diffraction limited spot of ∼200 nm diameter. The back-scattered fluorescence is long-pass-filtered, confocalized by a pinhole, and detected by an avalanche photodiode detector (APD, EG&G). The APD signal is fed into an auxiliary input channel of the AFM electronics.

Fluorescent polystyrene beads (40 nm) (FluoSpheres, Invitrogen) and 60 nm Au nanoparticles (BBI) are subsequently spread on a clean microscope cover slip by spin-coating and drop-casting methods, respectively. The 40 nm FSs contain ∼350 orange fluorophores (Invitrogen, Catalog No. F8792) with a quantum efficiency near unity (measured to be 98%). The final surface coverage is in the range of 0.1−0.5 particles/μm^2 and 0.5−5.0 particles/μm^2 for the FSs and AuNPs, respectively. The excitation and emission spectra of the 40 nm FS are shown in Figure 1b, lower panel. The laser wavelength of 532 nm (green vertical line) coincides with the absorption band of the fluorophore. The emission band of the fluorophore is centered around 560 nm at the peak maximum and extends to 650 nm. The extinction spectrum of an aqueous solution of 60 nm AuNPs (Figure 1b, upper panel) shows that the plasmon resonance band overlaps well with the emission spectrum of the fluorophore and the excitation wavelength. The sample surface is purged with a minute amount of nitrogen during the fluorescence measurement to avoid photo-oxidative bleaching effects on the fluorophores by ambient oxygen.

Figure 2 shows a sequence of AFM manipulation steps and corresponding fluorescence images (not every manipulation step is shown). The fluorescence images were taken with unpolarized illumination and collection. First, a proper pair of FSs is selected among a number of distributed FSs on the surface by help of the fluorescence image, and they are located in the simultaneously taken AFM images. The selection criterion is such that the chosen FSs do not neighbor AuNPs or other FSs in their immediate vicinities. One of the FSs (the right FS in the example shown in Figure 2) is kept untouched and serves as a reference during the entire experiment. A single AuNP is then approached toward the other FS (the left one in the example shown in Figure 2) in discreet AFM manipulation steps. After each manipulation step, the topography is scanned with the AFM. Subsequently, a fluorescence scan is carried out with the AFM cantilever retracted to ensure that the AFM tip does not influence the fluorescence. 3D representations of the topography around the left, sandwiched FS are displayed above each fluorescence image in Figure 2. In the fluorescence images, the luminescent spot on the right belongs to the reference FS, and the luminescent spot on the left belongs to the FS approached and sandwiched by the AuNPs. The left column in the figure shows in top-to-bottom sequence the approach of a first AuNP toward the FS from the right. The right column of Figure 2 shows the same FS while a second AuNP is brought toward the FS from the left such that two AuNPs sandwich the FS. In this way, a nanoscale gap bearing the single FS between the two AuNPs is formed. The fluorescence of the FS is enhanced with respect to the reference FS, indicating the formation of a hot spot.

The positions of the individual AuNPs and the FS are determined by taking height line cuts in the AFM topographic images along the sandwich axis. The central positions of the nanoparticles are found by Gaussian fits to the height data, and corresponding surface to surface distances between particle pairs are calculated by subtracting the radii of corresponding particles (as derived from the topographic height) from the center-to-center distances. The fluorescence enhancement is determined from the measured data after each manipulation step. The fluorescence strength, I_F, is found by integrating the signal over areas of 1.76 μm × 1.76 μm around the sandwiched FS, around the reference FS, and around an empty space for calculating background counts in the fluorescence images. Although precautions are taken to avoid photo-oxidative bleaching of the fluorophores in the FSs by purging the samples with N_2, a residual bleaching is always observed. Therefore, we normalize the background-subtracted fluorescence of the FS to be sandwiched, to the background-subtracted fluorescence of the reference FS to account for bleaching under the assumption that both FSs

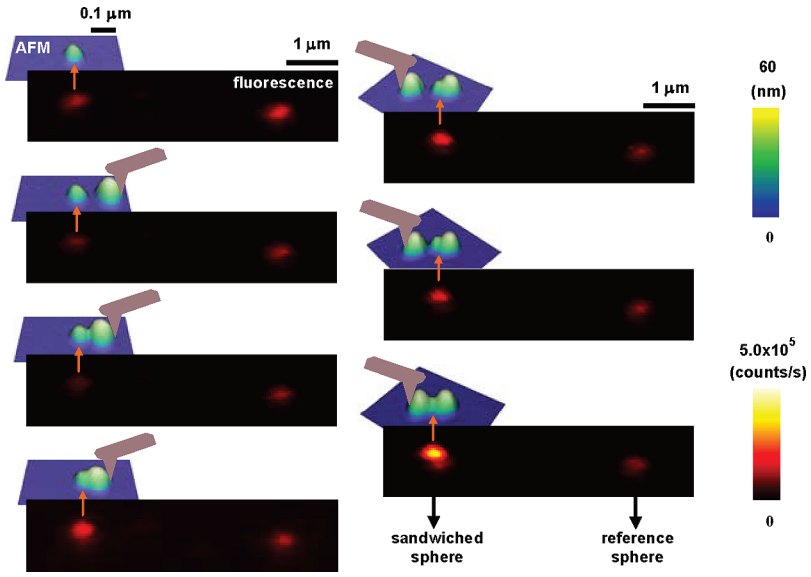

Figure 2. Series of manipulation steps. 3D AFM images of the sandwiched FS are displayed above each fluorescence image. In the fluorescence images, the luminescent spot on the right belongs to the reference FS, and the luminescent spot on the left belongs to the approached and sandwiched FS. The left column in the figure shows in top-to-bottom sequence the approach of a first AuNP toward the FS from the right; the right column shows the same FS as a second AuNP is brought toward the FS from the left such that two AuNPs sandwich the FS. When the sandwich is fully formed (in the last manipulation step), the fluorescence of the FS is substantially enhanced as compared to the reference FS.

bleach at the same rate. The integrated fluorescence strength I_F is then divided by the initial fluorescence strength I_F^0 taken before the first AuNP has been approached. The resulting quantity I_F/I_F^0 is called the normalized fluorescence enhancement.

Figure 3a shows the dependence of the normalized fluorescence enhancement on the AuNP−FS separation. The plot is divided into left and right parts by a vertical, dashed line. The left side of the plot shows the fluorescence enhancement as a function of the interparticle distance, d_1, during the approach of the first AuNP (see upper left sketch in the figure). During this approach, the fluorescence intensity initially decreases by 30% and reaches a minimum at a AuNP−FS distance of ∼90 nm. When the AuNP is approached even further, the fluorescence signal rises again, finally reaching 150% of the signal without AuNP (Figure 3a, left part). This dependence of the fluorescence enhancement on the single AuNP approach is similar to previous reports.[10,11] The right side of Figure 3a shows the fluorescence intensity as a function of the surface-to-surface distance, d_2, between two AuNPs as a second AuNP is approached from the opposite side, establishing thereby a AuNP−FS−AuNP sandwich (see upper right sketch in the figure). The fluorescence enhancement reaches a value of 2.72 (Figure 3a, right part), which is more than the simple product of two times the effect of a single AuNP ($1.5^2 = 2.25 < 2.72$). This indicates a hot spot effect, although the two AuNPs are still 40 nm apart, which is subideal for the formation of a strong hot spot. Nevertheless, the cooperative effect of two nanoparticles enhances the fluorescence more strongly than expected by two noninteracting AuNPs. A recent theoretical survey also found hot spot effects at AuNPs with larger separation.[34]

In a next series of experiments, we deliberately stopped the approach of the first AuNP at a distance of ∼(40 ± 10) nm; that is, at a distance, where the first AuNP quenches the fluorescence of the FS by 30% (Figure 3b). However, the subsequently approached second AuNP provokes an increase in the fluorescence intensity up to 2.15. This is less than in the case of the symmetrically assembled sandwich (2.72, right part of Figure 3a) but substantially more than a factor of 1.5 which is the maximum that can be achieved with a single fully approached AuNP (Figure 3a, left part). This is a remarkable result, because sandwiches consisting of a fully approached AuNP (which alone would increase the fluorescence by a factor of 1.5) and a AuNP separated by (40 ± 10) nm from the FS (which alone would result in a fluorescence quenching of 30%) show a net effect of a fluorescence increase by a factor of 2.15.

We have performed two further experiments that provide proof that the fluorescence enhancement is facilitated by the field enhancement in the center of the hot spot. First, we investigated the importance of the straight lineup of the three spheres. Figure 4a shows fluorescence intensities obtained from two different geometries. First, the geometry where all three particles are strictly lined up on a straight line, and second, a geometry where the FS is not on the line connecting the two AuNPs. The two upper insets show the AFM topographical images, and the two lower insets show the corresponding fluorescence images. The exact positions of the AuNPs and the FS are indicated by solid black dots and asterisks, respectively. The axis connecting the two AuNP centers is also indicated. In the case shown by the left insets, the FS is sandwiched straight between the two AuNPs, which leads to a strong fluorescence enhancement. The main graph of Figure 4a shows a line cut through the

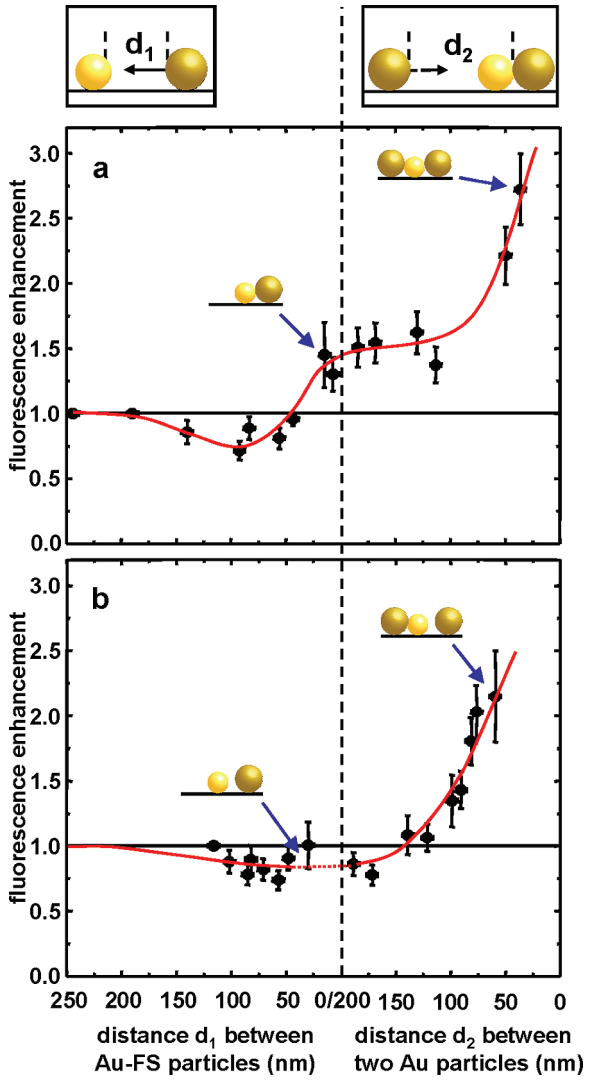

Figure 3. Fluorescence enhancement as a function of the distance, d_1, between the first AuNP and the FS (left side) and the distance, d_2, between the first and the second AuNP in a sandwich configuration (right side). The two sequences of the experiments are sketched in the boxes above the plots. The vertical dashed line separates the portions of the graphs that belong to the initial single AuNP approach (left) and the subsequent sandwich formation (right). (a) Both AuNPs are fully approached to the FS. When the first AuNP is approached, an initial decrease of fluorescence is followed by a fluorescence increase when the AuNP−FS distance is smaller than 40 nm. The approach of the second AuNP increases the fluorescence further. (b) The first AuNP has not fully approached the FS; the approach is stopped at a distance of ~40 nm. At this distance, the first AuNP acts as a quencher. When the second AuNP is approached, the fluorescence increases. Drawings in the plots display the situation around the data regions that are marked by arrows. The red curves are guides to the eye. The dashed part of the red line in part b indicates that the first particle has not been approached further. Two approach series are averaged for the data in part a, and three series are averaged in part b.

fluorescence profile, as indicated in the inset (red solid line). In the case of the two right insets, the FS is not in the hot spot, and consequently, the fluorescence enhancement is less pronounced (green broken line). The two fluorescence intensity profiles show that the fluorescence is enhanced only 1.27 times in the misaligned (green dashed line) and 2.72 times in the properly axially aligned sandwiches (red solid

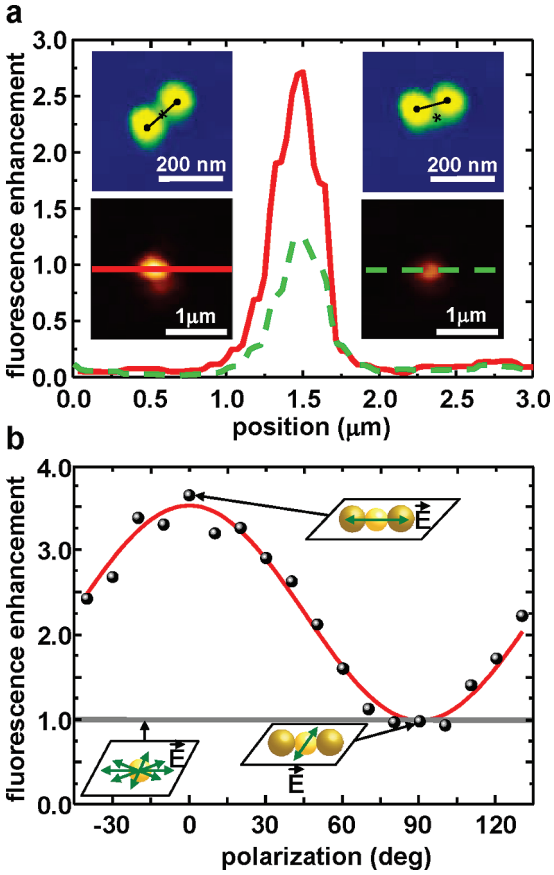

Figure 4. (a) The fluorescence enhancement is very sensitive to the exact placement of the FS between the AuNPs. The graph shows fluorescence intensities obtained with two different FS positions. The AFM height images are shown in the upper two insets, and the corresponding fluorescence images are shown in the lower two insets. The exact positions of the AuNPs and the FS are indicated by solid black dots and asterisks, respectively. The axis connecting the two AuNP centers is also indicated. In the left column, the FS is sandwiched in the hot spot right between the two AuNPs, which leads to a strong fluorescence enhancement (solid red line). In the right column, the FS is not in the hot spot, and consequently, the fluorescence enhancement is less pronounced (dashed green line). (b) The polarization of the excitation laser is rotated through 180°. The fluorescence intensity is enhanced when the laser is polarized parallel to the axis of the sandwich, whereas the fluorescence is decreased when the laser is polarized perpendicular to it. The gray horizontal line shows the fluorescence level of the FS before the AuNPs have been approached (using unpolarized excitation). The red curve is a $\sin^2$ fit to the data.

line). This sensitive dependence on the exact positioning of the FS in the AuNP sandwich proves that the hot spot is strongly localized between the two AuNPs.

In the second experiment (Figure 4b), the dependence of the fluorescence enhancement on the excitation polarization direction is shown. A maximal enhancement of 3.64 is observed at a polarization angle of 0°, corresponding to the sandwich axis. The observed minimum corresponds to a polarization that is orthogonal to the sandwich axis and shows no enhancement. The gray horizontal line shows the fluorescence level of the solitary FS with unpolarized excitation, and the red curve is a $\sin^2$ fit to the data. The excellent $\sin^2$ fit indicates that the dominant effect of the fluorescence enhancement is due to an enhanced excitation of the

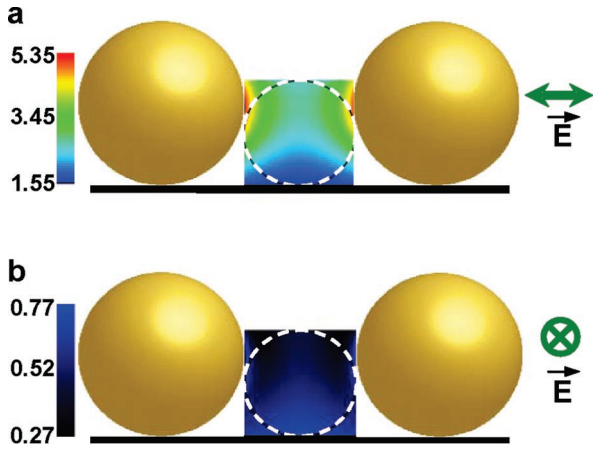

Figure 5. Calculated field enhancement (532 nm). (a) The electric field is enhanced for E-field polarization parallel to the dimer axis. (b) The electric field is suppressed for E-field polarization perpendicular to the dimer axis. The FS is indicated as a dashed line.

fluorophores (which must scale with the square of the electric field), whereas quenching of the fluorescence due to the neighboring gold nanoparticles is less important.[10,11,28]

To compare our results with theory, we calculated the near field of the 60 nm AuNP dimer at 532 nm (excitation wavelength) using generalized Mie theory.[35] For the sake of simplicity and computational cost, the electric field (E-field) is only calculated in a three-dimensional space that contains the FS, and the substrate is not taken into account (Figure 5). In the case of an E-field polarization parallel to the dimer axis, the field is increased up to a factor of 5.35 between the two AuNPs (Figure 5a), whereas the E-field is locally reduced down to a factor of 0.27 in the case of the perpendicular polarization. To compare our calculations with the experimental situation, we averaged the E-field over the whole volume of the 40 nm FS. Similarly, we calculated the averaged intensity enhancement, which is proportional to the square of the E-field. The volume-averaged electric field amplitude and intensity are calculated to enhance by a factor of 2.56 and 6.86, respectively, for the parallel polarization. In the case of the perpendicular polarization, the averaged E-field and intensity decrease by a factor of 0.60 and 0.37, respectively. These numerical results qualitatively agree with our experimental results (see Figure 4a). We would like to point out that the AuNP plasmon resonance only marginally shifts by <10 nm when the two AuNPs have been approached down to 40 nm distance. Therefore, the major contribution to the fluorescence enhancement is due to field enhancement rather than a spectral shift of the nanoparticle plasmon in or out of resonance with the fluorophore.

In conclusion, we have produced a fluorescence-enhancing hot spot by mechanically positioning two individual single gold nanoparticles around a fluorescent sphere and forming a sandwich. The formation of the hot spot manifests itself by a clear enhancement of the fluorescence signal from the fluorescent sphere as the interparticle distance between the gold nanoparticles forming the sandwich is reduced. The AFM manipulation technique can easily be extended to design more complicated arrangements of gold nanoparticles. Therefore, we expect that it will become a comprehensive tool for investigations whenever custom-designed arrangements of AuNPs matter. Examples are the better understanding of surface enhanced Raman scattering and hot-spot-enhanced fluorescence already mentioned in the introduction, but it also comprises very recent applications of gold nanoparticles in metamaterials[36,37] or also semiconductor nanocrystals in custom designed geometries, such as cascaded energy transfer structures.[38]

Acknowledgment. We thank Werner Stadler and Anna Helfrich for excellent technical assistance. This work has been supported by the Deutsche Forschungsgemeinschaft (DFG) through the SFB 486, the Gottfried-Wilhelm-Leibniz Program, and via the "Nanosystems Initiative Munich (NIM)".

References

(1) Purcell, E. M. *Phys. Rev.* **1946**, *69*, 681.
(2) Vuckovic, J.; Loncar, M.; Scherer, A. *IEEE J. Quant. Electron.* **2000**, *36*, 1131.
(3) Waks, E.; Inoune, K.; Santori, C.; Fattal, D.; Vuckovic, J.; Solomon, G. S.; Yamamoto, Y. *Science* **2002**, *420*, 762.
(4) Goy, P.; Raimond, J. M.; Gross, M.; Haroche, S. *Phys. Rev. Lett.* **1983**, *50*, 1903.
(5) Kiraz, A.; Michler, P.; Becher, C.; Gayral, B.; Imamoglu, A.; Zhang, L.; Hu, E.; Schoenfeld, W. V.; Petroff, P. M. *Appl. Phys. Lett.* **2001**, *78*, 3932.
(6) Yablonovitch, E. *Phys. Rev. Lett.* **1987**, *58*, 2059.
(7) Drexhage, K. H.; Kuhn, H.; Schäfer, F. P. *Ber. Buns.-Ges. Phys. Chem.* **1968**, *72*, 329.
(8) Barnes, W. L. *J. Mod. Opt.* **1998**, *45*, 661.
(9) Dulkeith, E.; Morteani, A. C.; Niedereichholz, T.; Klar, T. A.; Feldmann, J.; Levi, S. A.; van Veggel, F. C. J. M.; Reinhoudt, D. N.; Möller, M.; Gittins, D. I. *Phys. Rev. Lett.* **2002**, *89*, 203002.
(10) Anger, P.; Bharadwaj, P.; Novotny, L. *Phys. Rev. Lett.* **2006**, *96*, 113002.
(11) Kühn, S.; Hakanson, U.; Rogobete, L.; Sandoghdar, V. *Phys. Rev. Lett.* **2006**, *97*, 017402.
(12) Tam, F.; Goodrich, G. P.; Johnson, B. R.; Halas, N. J. *Nano Lett.* **2007**, *7*, 496.
(13) Fleischmann, M.; Hendra, P. J.; McQillian, A. J. *Chem. Phys. Lett.* **1974**, *26*, 163.
(14) Albrecht, M. G.; Creighton, J. A. *J. Am. Chem. Soc.* **1977**, *99*, 5215.
(15) Jeanmarie, D. L.; Van Duyne, R. P. *J. Electroanal. Chem.* **1977**, *84*, 1.
(16) Kneipp, K.; Yang, W.; Kneipp, H.; Perelman, L. T.; Itzkan, I.; Dasari, R. R.; Feld, M. S. *Phys. Rev. Lett.* **1997**, *78*, 1667.
(17) Nie, S.; Emory, S. R. *Science* **1997**, *275*, 1102.
(18) Chen, C. Y.; Burstein, E. *Phys. Rev. Lett.* **1980**, *45*, 1287.
(19) Arias, J.; Aravind, P. K.; Metiu, H. *Chem. Phys. Lett.* **1982**, *85*, 404.
(20) Lakowicz, J. R. *Anal. Biochem.* **2001**, *298*, 1.
(21) Hillenbrand, R.; Keilmann, F. *Appl. Phys. B* **2001**, *73*, 239.
(22) Xu, H. X.; Bjerneld, E. J.; Käll, M.; Börjesson, L. *Phys. Rev. Lett.* **1999**, *83*, 4357.
(23) Xu, H.; Käll, M. *ChemPhysChem* **2003**, *4*, 1001.
(24) Talley, C. E.; Jackson, J. B.; Oubre, C.; Grady, N. K.; Hollars, C. W.; Lane, S. M.; Huser, T. R.; Nordlander, P.; Halas, N. J. *Nano Lett.* **2005**, *5*, 1569.
(25) Olk, P.; Renger, J.; Härtling, T.; Wenzel, M. T.; Eng, L. M. *Nano Lett.* **2007**, *7*, 1736.
(26) Ringler, M.; Klar, T. A.; Schwemer, A.; Susha, A. S.; Stehr, J.; Raschke, G.; Funk, S.; Borowski, M.; Nichtl, A.; Kürzinger, K.; Phillips, R. T.; Feldmann, J. *Nano Lett.* **2007**, *7*, 2753−2757.
(27) Farahani, J. N.; Pohl, D. W.; Eisler, H. J.; Hecht, B. *Phys. Rev. Lett.* **2005**, *95*, 017402.
(28) Muskens, O. L.; Giannini, V.; Sanchez-Gil, J. A.; Gomez Rivas, J. *Nano Lett.* **2007**, *7*, 2871−2875.
(29) Zhang, J.; Fu, Y.; Chowdhury, M. H.; Lakowicz, J. R. *Nano Lett.* **2007**, *7*, 2101.

(30) Fromm, D. P.; Sundaramurthy, A.; Schuck, P. J.; Kino, G.; Moerner, W. E. *Nano Lett.* **2004**, *4*, 957.
(31) Schaefer, D. M.; Reifenberger, R.; Patil, A.; Andres, R. P. *Appl. Phys. Lett.* **1995**, *66*, 1012.
(32) Junno, T.; Deppert, K.; Montelius, L.; Samuelson, L. *Appl. Phys. Lett.* **1995**, *66*, 3627.
(33) Kassies, R.; van der Werf, K. O.; Lenferink, A.; Hunter, C. N.; Olsen, J. D.; Subrahmanyam, V.; Otto, C. *J. Microsc.* **2005**, *217*, 109.
(34) Dahmen, C.; Schmidt, B.; von Plessen, G. *Nano Lett.* **2007**, *7*, 318.
(35) Xu, Y. *Appl. Opt.* **1995**, *34*, 4573.
(36) Podolskiy, V. A.; Sarychev, A. K.; Shalaev, V. M. *J. Nonlinear Opt. Phys. Mater.* **2002**, *11*, 65.
(37) Engheta, N.; Salandrino, A.; Alu, A. *Phys. Rev. Lett.* **2005**, *95*, 095504.
(38) Franzl, T.; Klar, T. A.; Schietinger, S.; Rogach, A. L.; Feldmann, J. *Nano Lett.* **2004**, *4*, 1599.

NL072602N